

A Mathematical Model of Tripartite Synapse: Astrocyte Induced Synaptic Plasticity

Shivendra Tewari

shivendra@isibang.ac.in

*Systems Science and Informatics Unit
Indian Statistical Institute
8th Mile, Mysore Road
Bangalore 560059, India*

Kaushik Majumdar

kmajumdar@isibang.ac.in

*Systems Science and Informatics Unit
Indian Statistical Institute
8th Mile, Mysore Road
Bangalore 560059, India*

In this paper we present a mathematical model of tripartite synapses, where astrocytes mediate information flow from the pre-synaptic to the post-synaptic neuron. The model consists of a pre-synaptic bouton, a post-synaptic dendritic spine head, a synaptic cleft and a perisynaptic astrocyte controlling Ca^{2+} dynamics inside the synaptic bouton. This in turn controls glutamate release dynamics in the cleft. As a consequence of this, glutamate concentration in the cleft has been modeled, in which glutamate reuptake by astrocytes has also been incorporated. Finally, dendritic spine head dynamics has been modeled. As an application, this model clearly shows synaptic potentiation in the hippocampal region, i.e., astrocyte Ca^{2+} mediates synaptic plasticity, which is in conformity with the majority of the recent findings.

1. Introduction

One of the most significant challenges in neuroscience is to identify the cellular and molecular processes that underlie learning and memory formation (Lynch, 2004). Cajal originally hypothesized that information storage relies on changes in strength of synaptic connections between neurons that are active (Cajal, 1913). Hebb supported this hypothesis and proposed that if two neurons are active at the same time, the synaptic efficiency of the appropriate synapse will be strengthened (Hebb, 1949). Synaptic transmission is a dynamic process. Post-synaptic responses wax and wane as pre-synaptic activity evolves. Forms of synaptic enhancement, such as facilitation, augmentation, and post-tetanic potentiation, are usually attributed to effects of a residual elevation in pre-synaptic Ca^{2+} concentration ($[\text{Ca}^{2+}]$), acting on one or more molecular targets that appear to be distinct from the secretory trigger responsible for fast exocytosis and phasic release

of transmitter to single action potential (Zucker & Regehr, 2002). It is now well established that the astrocytic mGluR detects synaptic activity and responds via activation of the calcium-induced calcium release pathway, leading to elevated Ca^{2+} levels. The spread of these levels within micro-domain of one cell can coordinate the activity of disparate synapses that are associated with the same micro-domain (Perea & Araque, 2002). The notion of tripartite synapse consisting of pre-synaptic neuron, post-synaptic neuron and astrocyte has taken a firm root in experimental (Araque, et al., 1999; Newman, 2003; Perea & Araque, 2007) as well as theoretical neuroscience (Nadkarni & Jung, 2003; Volman et al., 2007; Nadkarni, et al., 2008). Astrocytes play crucial roles in the control of Hebbian plasticity (Fellin, 2009).

There is a recent report, that at least in the hippocampus, astrocyte Ca^{2+} signaling does not modulate short-term or long-term synaptic plasticity (Agulhon, et al., 2010). However evidences of astrocytic modulation of synaptic plasticity are more abundant including in hippocampus (Vernadakis, 1996; Haydon, 2001; Yang et al., 2003; Andersson, 2010; Henneberger, et al., 2010). Neuronal activities can trigger Ca^{2+} elevations in astrocytes (Porter & McCarthy, 1996; Fellin, 2009) leading to concentration increases in adjacent glial cells including astrocytes, which expresses a variety of receptors (Newman, 2003). These activated receptors increase astrocyte $[\text{Ca}^{2+}]$, and release transmitters, including glutamate, D-serine, ATP (Parpura et al., 1994; Henneberger et al., 2010) etc. The released gliotransmitters feed-back onto the pre-synaptic terminal either to enhance or to depress further release of neurotransmitter (Newman, 2003) including glutamate, which is mediated by Ca^{2+} concentration in the pre-synaptic terminal. It is worthy to note that Ca^{2+} elevations are both necessary and sufficient to evoke glutamate release from astrocytes (Haydon, 2001). On the other hand short-term synaptic depression is caused by depletion of the releasable vesicle pool due to recent release in response to pre-synaptic action potential (Wu & Borst, 1999). This entire chain of Ca^{2+} mediated pre-synaptic activity consisting of both short-term enhancement (STE) and short-term depression (STD) can be called short-term synaptic plasticity or simply short-term plasticity (STP).

Synaptic plasticity occurs at many time scales. Usually long-term plasticity (LTP) happens at a time scale of 30 minutes or more and STP takes less than that (p – 311, Koch, 1999). Within the ambit of STP, STE has been more widely studied than the STD. A quantitative definition of STE has been proposed in (Fisher et al., 1997). STE has been divided into four different temporal regimes, namely fast-decaying facilitation (10s of milliseconds), slow-decaying facilitation (100s of milliseconds), augmentation (seconds) and post-tetanic potentiation (minutes) (Fisher et al., 1997).

STP is thought to provide a biological mechanism for on-line information processing in the central nervous system (Fisher et al., 1997) and therefore could be the key to the formation of working memory and intelligent behavior. A computational model of how cellular and molecular dynamics give rise to the STP in the synapses (particularly in the

synapses of the hippocampus and the prefrontal cortex) can be quite useful in understanding intelligent behavior.

In this paper, we present a computational model of astrocyte mediated augmentation in a tripartite synapse. The following steps have been followed in simulation of our model. (1) Pre-synaptic action potential train has been generated using the Hodgkin-Huxley model (Hodgkin & Huxley, 1952). (2) Ca^{2+} concentration elevation in the pre-synaptic bouton. (3) Glutamate release enhancement in the synaptic cleft. (4a) Glutamate modulated enhancement of astrocytic Ca^{2+} . (4b) Glutamate mediated excitatory post-synaptic potential. (5) Extra-synaptic glutamate elevation as a consequence of (4a). On measuring the windowed average amplitude of the excitatory post-synaptic current (EPSC) we could observe up to 250% increase from pre-astrocytic activities to the post-astrocytic activities, which decayed with a time constant of 10 to 12 seconds. This signifies augmentation (Fisher et al., 1997; Koch, 1999).

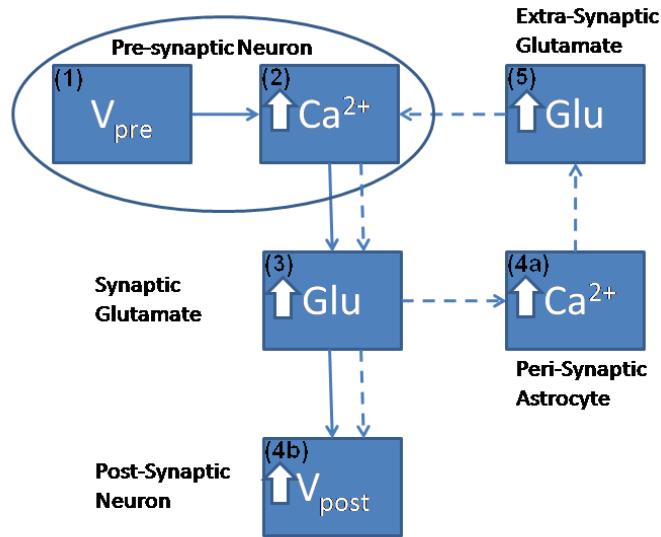


Figure 1. Information flow from pre-synaptic bouton to post-synaptic dendrite spine-head, as modulated by an astrocyte. Solid line shows the astrocyte-independent pathway, while, solid-line combined with dashed line shows the astrocyte-dependent pathway. (1) AP generated at pre-synaptic axon-hillock. (2) Elevated intracellular $[\text{Ca}^{2+}]$ in bouton. (3) Increased $[\text{Ca}^{2+}]$ leading to exocytosis of Glutamate into synaptic cleft. (4a) Synaptic glutamate causes an increase in astrocyte $[\text{Ca}^{2+}]$. (4b) Simultaneously, synaptic glutamate can also bind with AMPAR causing an increase in post-synaptic membrane potential. (5) Increased astrocyte $[\text{Ca}^{2+}]$ leads to an elevated glutamate concentration in the extra-synaptic cleft, in a vesicular dependent manner. This extra-synaptic glutamate is free to bind with extra-synaptic mGluR on the pre-synaptic bouton surface. $\text{Glu} \cdot \text{mGluR}$ leads to an increase in Ca^{2+} concentration via IP_3 dependent pathway. This

transient enhancement of bouton $[Ca^{2+}]$, forms the basis of improved synaptic efficacy, through an astrocyte-dependent pathway.

2. The Model

In this section, we describe the details of the mathematical model, whose computational implementation will be presented in the section that immediately follows. In order to elucidate the major neurophysiological steps in our model we use the flow chart in Figure 1. The mathematical formulations have been described in the subsequent subsections.

2.1 Pre-synaptic Action Potential

Action potential (AP) is generated at the axon hillock of the pre-synaptic neuron. In the cortical neurons there may be eleven or more number of different ion channels (Lytton & Sejnowski, 1991). Key features of initiation dynamics of cortical neuron APs – their rapid initiation and variable onset potential – are outside the range of behaviors described by the classical Hodgkin-Huxley (HH) theory (Naundorf et al., 2006). Still the HH paradigm has been used to generate pre-synaptic AP in computational models (Nadkarni & Jung, 2003; Volman et al., 2007). Since in this paper our focus is not on the detail of the pre-synaptic AP generation, for the sake of simplicity here we have followed the HH model for the pre-synaptic regular spikes and bursts generation.

$$\begin{aligned} C \frac{dV_{pre}}{dt} &= I_{app} - g_K n^4 (V_{pre} - V_K) - g_{Na} m^3 h (V_{pre} - V_{Na}) - g_L (V_{pre} - V_L) \\ \frac{dx}{dt} &= \alpha_x (1-x) - \beta_x x \end{aligned} \quad (1)$$

where V_{pre} is pre-synaptic membrane potential in millivolts, I_{app} is applied current density, g_K , g_{Na} and g_L are potassium, sodium and leak conductance respectively, V_K , V_{Na} and V_L are potassium, sodium and leak reversal potential respectively, and $x=m$ (Na^+ activation), h (Na^+ inactivation) and n (K^+ activation). The detail of the HH model can be found in (Hodgkin & Huxley, 1952). The values of the different parameters in equation (1) that have been used in this paper are furnished in the Table 1. α_x and β_x for $x = m$, h and n are defined as

$$\begin{aligned} \alpha_n &= \frac{0.01(-V_{pre} - 60)}{\exp\left(\frac{-V_{pre} - 60}{10}\right) - 1}, \alpha_m = \frac{0.1(-V_{pre} - 45)}{\exp\left(\frac{-V_{pre} - 45}{10}\right) - 1}, \alpha_h = 0.07 \exp\left(\frac{-V_{pre} - 70}{20}\right), \\ \beta_n &= 0.125 \exp\left(\frac{-V_{pre} - 70}{80}\right), \beta_m = 4 \exp\left(\frac{-V_{pre} - 70}{18}\right), \beta_h = \frac{1}{\exp\left(\frac{-V_{pre} - 40}{10}\right) + 1} \end{aligned}$$

Table 1: Parameter values used in the HH model (all are from Hodgkin & Huxley, 1952)

Symbol	Value
g_K	36 mS cm ⁻²
g_{Na}	120 mS cm ⁻²
g_L	0.3 mS cm ⁻²
V_K	-12 mV
V_{Na}	115 mV
V_L	10.6 mV

2.2 Bouton Ca²⁺ Dynamics

The train of AP that has been generated in the axon hillock of the pre-synaptic neuron, travels all the way down to the axon end feet without degradation and leads to an increase in cytosolic [Ca²⁺]. The increase in intracellular [Ca²⁺] can be attributed to two components:

- i) [Ca²⁺] due to AP, denoted as c_{fast} , and
- ii) [Ca²⁺] due to intracellular stores, c_{slow} .

Because of its rapid kinetics, [Ca²⁺] due to AP is termed as c_{fast} . Similarly, [Ca²⁺] due to intracellular stores is termed as, c_{slow} . Total intracellular [Ca²⁺], denoted as c_i satisfies the following simple equation,

$$c_i = c_{\text{fast}} + c_{\text{slow}}$$

The sensitivity of rapidly decaying Ca²⁺ kinetics over neuro-transmitter release is well established (Schneggenburger & Neher, 2000; Bollman et al. 2000). In immature neurons, the necessary Ca²⁺ flux for neurotransmitter release is primarily mediated by N-type Ca²⁺ channels (Mazzanti & Haydon, 2003; Weber et al. 2010). The equation governing c_{fast} consists of simple construction-destruction type formulism and is as follows (Keener & Sneyd, 1998),

$$\frac{dc_{\text{fast}}}{dt} = - \underbrace{\frac{I_{Ca} \cdot A_{btn}}{z_{Ca} F V_{btn}}}_{\text{construction}} + J_{PMleak} - \underbrace{\frac{I_{PMCa} \cdot A_{btn}}{z_{Ca} F V_{btn}}}_{\text{destruction}} \quad (2)$$

Here, I_{Ca} is the Ca²⁺ current through N-type channel, A_{btn} is the surface area of the bouton, z_{Ca} is the Ca²⁺ ion valence, F is the Faraday's constant, V_{btn} is the volume of the

bouton. I_{PMCa} represents the current due to electrogenic plasma-membrane Ca^{2+} ATPase. This pump is known to extrude excess of Ca^{2+} out of the cell and it has also been shown that it regulates excitatory synaptic transmission at CA3-CA1 synapse (Jensen et al., 2007). The formulation for this pump uses the standard Michaelis-Menton (MM) type formulism (Erler et al., 2004; Blackwell, 2005). J_{PMleak} is the positive leak from extracellular space into bouton, which makes sure that MM pump does not decrease cytosolic Ca^{2+} to 0 (Blackwell, 2005).

The Ca^{2+} current through the N-type Ca^{2+} channel is formulated using single protein level formulation, which is described elsewhere (Erler et al. 2004),

$$I_{Ca} = \rho_{Ca} m_{Ca}^2 \underbrace{g_{Ca}(V_{pre}(t) - V_{Ca})}_{\text{Single open channel}}$$

Here, ρ_{Ca} is the N-type channel protein density, g_{Ca} is the single N-type channel conductance, V_{Ca} is the reversal potential of Ca^{2+} ion determined by the Nernst equation (Keener & Sneyd, 1998),

$$V_{Ca} = \frac{RT}{z_{Ca}F} \ln \left(\frac{c_{\text{ext}}}{c_i^{\text{rest}}} \right)$$

Where, R is the real gas constant, T is the absolute temperature, c_{ext} is the extracellular Ca^{2+} concentration, c_i^{rest} is the total intracellular $[\text{Ca}^{2+}]$ at rest. It is assumed that a single N-type channel consists of two-gates. m_{Ca} denotes the opening probability of a single gate. A single N-type channel is open only when both the gates are open. Hence, m_{Ca}^2 is the single channel open probability. The time dependence of the single channel open probability is governed by a HH-type formulation,

$$\frac{dm_{Ca}}{dt} = \frac{(m_{Ca}^\infty - m_{Ca})}{\tau_{m_{Ca}}}$$

Where, m_{Ca}^∞ is the Boltzmann-function fitted by Ishikawa et al. (2005) to the whole cell current of an N-type channel, m_{Ca} approaches its asymptotic value m_{Ca}^∞ with a time constant $\tau_{m_{Ca}}$. The mathematical expression of other parameters used in equation (2) is as follows:

$$I_{PMCa} = v_{PMCa} \frac{c_i^2}{c_i^2 + K_{PMCa}^2}, J_{PMleak} = v_{leak} (c_{ext} - c_i), m_{Ca}^\infty = \frac{1}{1 + \exp((V_{m_{Ca}} - V_m) / k_{m_{Ca}})}$$

The parameter values used for simulation are listed in Table 2.

Table 2: Parameters used for Bouton Ca²⁺ dynamics

Symbol	Description	Value	Reference
F	Faraday's constant	96487 C mole ⁻¹	Known fact
R	Real gas constant	8.314 J / K	Known fact
T	Absolute Temperature	293.15 K	Assumed
z_{Ca}	Calcium valence	2	Known fact
A_{btm}	Surface area of bouton	1.24 μm ²	Calculated
V_{btm}	Volume of bouton	0.13 μm ³	Koester & Sakmann, 2000
ρ_{Ca}	N-type channel density	3.2 μm ⁻²	Adjusted
g_{Ca}	N-type channel conductance	2.8 pS	Weber et al. 2010
V_{Ca}	Reversal potential of Ca ²⁺ ion	125 mV	Calculated
v_{PMCa}	Maximum PMCa current	0.4 μA cm ⁻²	Adjusted
K_{PMCa}	Ca ²⁺ concentration at which v_{PMCa} is halved	0.1 μM	Erler et al. 2004
v_{leak}	Maximum leak of Ca ²⁺	2.66 x 10 ⁻⁶ ms ⁻¹	Calculated
c_i^{rest}	Resting Intracellular Ca ²⁺ concentration	0.1 μM	Assumed
c_{ext}	External Ca ²⁺ concentration	2 mM	Assumed
V_{mCa}	Half-activation voltage of N-type Ca ²⁺ channel	-17 mV	Ishikawa et al. 2005
k_{mCa}	Slope factor of N-type channel activation	8.4 mV	Ishikawa et al. 2005
c_1	Ratio of ER volume to volume of Bouton	0.185	Shuai & Jung, 2002
v_1	Maximum IP ₃ receptor flux	30 s ⁻¹	Modified from Jafri & Keizer, 1995
v_2	Ca ²⁺ leak rate constant	0.055 s ⁻¹	Modified from Shuai & Jung, 2002
v_3	SERCA maximal pump rate	90 μM s ⁻¹	Modified from Jafri & Keizer, 1995
k_3	SERCA dissociation constant	0.1 μM	Jafri & Keizer, 1995
d_1	IP ₃ dissociation constant	0.13 μM	Shuai & Jung, 2002
d_2	Inhibitory Ca ²⁺ dissociation constant	1.049 μM	Shuai & Jung, 2002
d_3	IP ₃ dissociation constant	943.4 nM	Shuai & Jung, 2002
d_5	Activation Ca ²⁺ dissociation constant	82.34 nM	Shuai & Jung, 2002
a_2	Inhibitory Ca ²⁺ binding constant	0.2 μM s ⁻¹	Shuai & Jung, 2002
v_g	Maximum production rate of IP ₃	0.7 nM ms ⁻¹	Modified from Nadkarni & Jung, 2007
k_g	Glutamate concentration at which v_g is halved	785 nM	Nadkarni & Jung, 2007

τ_p	IP ₃ degradation constant	0.14 s ⁻¹	Nadkarni & Jung, 2007
p_0	Initial IP ₃ concentration	160 nM	Nadkarni & Jung, 2007

The second component of bouton Ca²⁺, c_{slow} , is the slower component. It is known to play a crucial role in STP (Emptage et al., 2001). The release of Ca²⁺ from endoplasmic reticulum (ER) is mainly controlled by two types of receptors (or Ca²⁺ channels) i) the inositol (1,4,5)-trisphosphate receptor (IP₃R) and ii) the ryanodine receptor (RyR) (Sneyd & Falcke, 2005). For the sake of simplicity, the flow is assumed to be through IP₃R alone. The IP₃ necessary for release of Ca²⁺ from ER, is produced when glutamate (agonist) binds with mGluR (receptor) and causes via G-protein link to phospholipase C (PLC), the cleavage of phosphatidylinositol (4,5)-bisphosphate (PIP₂) to produce IP₃ and diacylglycerol (DAG). We have used the conventional Li-Rinzel model (L-R model) (Li & Rinzel, 1994) to formulate this slower Ca²⁺ signaling process. There were a few modifications made to the L-R model. The L-R model assumes that, total intracellular concentration, c_0 , is conserved and determines the ER Ca²⁺ concentration, c_{ER} , using the following relation,

$$c_{\text{ER}} = \frac{(c_0 - c_i)}{c_1}$$

Such an assumption is not valid in the present model because of the presence of membrane fluxes, namely, I_{Ca} and I_{PMCa} . Also, in the L-R model intracellular IP₃ concentration is used as a control parameter. To take care of these “inconveniences” two additional equations governing ER [Ca²⁺] and [IP₃] have been incorporated in the L-R model. The [IP₃] production term was made glutamate dependent to study the effect of astrocytic Ca²⁺ over c_i (Nadkarni & Jung, 2007). The mathematical model governing the c_{slow} dynamics is as follows,

$$\begin{aligned} \frac{dc_{\text{slow}}}{dt} &= -J_{\text{chan}} - J_{\text{ERpump}} - J_{\text{ERleak}} \\ \frac{dc_{\text{ER}}}{dt} &= -\frac{1}{c_1} \frac{dc_{\text{slow}}}{dt} \\ \frac{dp}{dt} &= v_g \frac{g_a^{0.7}}{k_g^{0.7} + g_a^{0.7}} - \frac{1}{\tau_p} (p - p_0) \\ \frac{dq}{dt} &= \alpha_q (1 - q) - \beta_q q \end{aligned} \quad (3)$$

Here, J_{chan} denotes Ca²⁺ flux from ER to the intracellular space through IP₃R, J_{ERpump} is the Ca²⁺ flux pumped from the intracellular space into ER, J_{ERleak} is the leak of Ca²⁺ ions

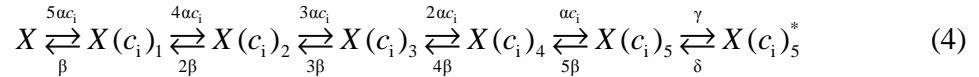
from ER to intracellular space, c_{ER} is the ER Ca^{2+} concentration, c_i is the ratio of volume of ER to volume of bouton, p is the intracellular IP_3 concentration, g_a is the glutamate in the extra-synaptic cleft, q is the fraction of activated IP_3R . The expressions for the fluxes is,

$$\begin{aligned} J_{\text{chan}} &= c_i v_1 m_\infty^3 n_\infty^3 q^3 (c_i - c_{\text{ER}}) \\ J_{\text{ERpump}} &= \frac{v_3 c_i^2}{k_3^2 + c_i^2} \\ J_{\text{ERleak}} &= c_i v_2 (c_i - c_{\text{ER}}) \end{aligned}$$

With, $m_\infty = \frac{p}{p + d_1}$, $n_\infty = \frac{c_i}{c_i + d_5}$, $\alpha_q = a_2 d_2 \frac{p + d_1}{p + d_3}$, $\beta_q = a_2 c_i$. Details of parameters are as listed in Table 2.

2.3 Glutamate release dynamics in bouton

It is now widely accepted that AP waveforms lead to a transient increase in intracellular $[\text{Ca}^{2+}]$ and leads to neurotransmitter release (Bollman et al. 2000; Wang et al., 2009). However, the study of Ca^{2+} sensor sensitivity becomes exceedingly challenging due to small size of nerve terminals (Wang et al., 2009). It is generally assumed that Ca^{2+} concentration of at least 100 μM in the terminal is necessary for a “low-affinity” Ca^{2+} sensor to activate (Neher, 1998; Nadkarni & Jung, 2008). But, recent studies performed at giant Calyx of Held terminal have revealed that intracellular Ca^{2+} concentration of $\sim 10 \mu\text{M}$ is sufficient for glutamate release (Schneggenburger & Neher, 2000; Bollman et al., 2000). The kinetic model governing the Ca^{2+} binding to Ca^{2+} sensor is given by the following equations (Bollman et al., 2000),



Where, α and β are the Ca^{2+} association and dissociation rate constants, respectively; γ and δ are Ca^{2+} independent isomerisation constants. X is the Ca^{2+} sensor with no Ca^{2+} bound, $X(c_i)_1$ is Ca^{2+} sensor with one Ca^{2+} bound, likewise, $X(c_i)_5$ is Ca^{2+} sensor with five Ca^{2+} bound; $X(c_i)_5^*$ is the isomer of $X(c_i)_5$ which is ready for glutamate release. Hippocampal synapses are known as low-fidelity synapses (Nadkarni & Jung, 2008). We have assumed an active zone consisting of two-docked synaptic vesicle (Danbolt, 2001; Nikonenko & Skibo, 2006). Since, there are few synaptic vesicles; the release process cannot be determined by the average release rate. Therefore, vesicle release probability,

P_r , has been determined using dynamic Monte-Carlo simulation (Fall et al., 2002) of kinetic equation (4). The vesicle fusion and recycling process is governed by the Tsodyks & Markram model (Tsodyks & Markram, 1997). A slight modification has been made to the Tsodyks & Markram Model (TMM) to make the vesicle fusion process ' P_r ' dependent. The modified TMM is as follows,

$$\begin{aligned}\frac{dR}{dt} &= \frac{I}{\tau_{\text{rec}}} - P_r \cdot R \\ \frac{dE}{dt} &= -\frac{E}{\tau_{\text{inact}}} + P_r \cdot R \\ I &= 1 - R - E\end{aligned}\quad (5)$$

Where, 'R' is the fraction of releasable vesicles inside bouton, 'E' is the fraction of effective vesicles in the synaptic cleft and 'I' is the fraction of inactive vesicles undergoing recycling process; P_r has the value (0, 0.5, 1) corresponding to the number of vesicles ready to be released (0, 1, 2), which is determined by the stochastic simulation of kinetic model in equation (4); τ_{inact} and τ_{rec} are the time constants of vesicle inactivation and recovery, respectively.

Apart from evoked release of glutamate, spontaneous release of glutamate can also occur. The rate of spontaneous release depends upon pre-synaptic Ca^{2+} concentration (Emptage et al., 2001; Nadkarni & Jung, 2008). The spontaneous release of glutamate is assumed to be a Poisson process with the following rate (Nadkarni & Jung, 2008),

$$\lambda(c_i) = a_3 \left(1 + \exp\left(\frac{a_1 - c_i}{a_2}\right) \right)^{-1}$$

Once a vesicle is released whether evoked or spontaneous, the vesicle release process remains inactivated for a period of 6.34 ms (Nadkarni & Jung, 2008). The parametric values used for simulation are listed in Table 3.

2.4 Glutamate dynamics in synaptic cleft

Various types of glutamate receptors have been detected pre-synaptically, extra-synaptically, as well as on glial cells (Danbolt, 2001). Suggesting that, to study transmission of glutamatergic signals, it is essential to study, how glutamate diffuses (Danbolt, 2001). However, using Monte Carlo simulation of a central glutamatergic synapse, in particular CA3–CA1 synapse, Franks et al., (2002) showed that glutamatergic signaling is spatially independent at these synapses. The capacity of the bouton vesicle containing glutamate has been assumed to be 60 mM (Danbolt, 2001). Since, E gives the

effective fraction of vesicles in the cleft; the estimated glutamate concentration in the cleft can be represented mathematically as,

$$\frac{dg}{dt} = n_v \cdot g_v \cdot E - g_c \cdot g \quad (6)$$

Here, g is the glutamate concentration in the synaptic cleft, n_v is the number of docked vesicle, g_v is the vesicular glutamate concentration and g_c is the rate of glutamate clearance i.e. re-uptake by neuron or astrocyte (Destexhe et al., 1998). Using this simple dynamics, we could achieve the estimated range of glutamate concentration 0.24 - 11 mM in cleft (Danbolt, 2001; Franks et al., 2002) and time course of glutamate in the cleft 2 ms (Franks et al., 2002; Nadkarni & Jung, 2007). Although similar equation can be used to model glutamate dynamics at other synapses, however, one might have to use different constant values. Thus, the present formulation can be considered specific to a CA3 – CA1 synapse.

Table 3: Parameters used for Glutamate dynamics in bouton and cleft

Symbol	Description	Value	Reference
α	Ca ²⁺ association rate constant	0.3 μM ms ⁻¹	Bollman et al. 2000
β	Ca ²⁺ dissociation rate constant	3 ms ⁻¹	Bollman et al. 2000
γ	Isomerization rate constant (forward)	30 ms ⁻¹	Bollman et al. 2000
δ	Isomerization rate constant (backward)	8 ms ⁻¹	Bollman et al. 2000
τ_{rec}	Vesicle recovery time constant	800 ms	Tsodyks & Markram, 1997
τ_{inac}	Vesicle inactivation time constant	3 ms	Tsodyks & Markram, 1997
a_1	Ca ²⁺ concentration at which λ is halved	2700 nM	Modified from Nadkarni & Jung, 2008
a_2	Slope factor of spontaneous release rate λ	305 nM	Modified from Nadkarni & Jung, 2008
a_3	Maximum spontaneous release rate	100 ms ⁻¹	Nadkarni & Jung, 2008
n_v	Number of docked vesicle	2	Nikonenko & Skibo, 2006
g_v	Glutamate concentration in single vesicle	60 mM	Montana et al., 2006
g_c	Glutamate clearance rate constant	10 ms ⁻¹	Destexhe et al., 1998

2.5 Astrocyte Ca²⁺ dynamics

Porter & McCarthy (1996) showed that glutamate released from the Schaffer collaterals leads to an increase in astrocytic Ca²⁺ via an mGluR pathway. Recently, Pitta et al.

(2009) proposed a G-Chi model for astrocytic Ca^{2+} oscillations mediated by mGluR pathway while treating glutamate, g , as a parameter. We have used the G-Chi model for astrocyte Ca^{2+} dynamics with an exception that ‘ g ’ is a dynamic variable given by equation (6). The G-Chi model uses the conventional L-R model for astrocytic Ca^{2+} concentration ‘ c_a ’ with some specific terms for intracellular IP_3 concentration ‘ p_a ’. The G-Chi model is a closed-cell model (Keener & Sneyd, 2009) i.e. without membrane fluxes. In such models, c_a , primarily depends upon two parameters, i) Flux from ER into cytosol and ii) The maximal pumping capacity of the Sarco-Endoplasmic Reticulum ATPase (SERCA) pump. It is known that IP_3 Rs are found in clusters in astrocytes (Nadkarni & Jung, 2007). However, the size of the cluster, N_{IP_3} , is not known we have assumed it to be ‘20’ (Shuai & Jung, 2002; Nadkarni & Jung, 2007). Considering, such small cluster “stochasticity” becomes inevitable (Shuai & Jung, 2002). We make use of the stochastic L-R model (Shuai & Jung, 2002). The model can be represented as follows:

$$\begin{aligned} \frac{dc_a}{dt} &= \left(r_{c_a} m_\infty^3 n_\infty^3 h^3 + r_L \right) \left(c_0 - \left(1 + c_{1,a} \right) c_a \right) - v_{\text{ER}} \frac{c_a^2}{c_a^2 + K_{\text{ER}}^2} \\ \frac{dp_a}{dt} &= v_\beta \cdot \text{Hill} \left(g^{0.7}, K_R \left(1 + \frac{K_p}{K_R} \text{Hill}(C, K_\pi) \right) \right) + \frac{v_\delta}{1 + \frac{p_a}{k_\delta}} \text{Hill}(c_a^2, K_{\text{PLC}\delta}) \\ &\quad + v_{3K} \text{Hill}(c_a^4, K_D) \text{Hill}(p_a, K_3) - r_{5p_a} p_a \\ \frac{dh}{dt} &= \frac{h_\infty - h}{\tau_h} + G_h(t) \end{aligned} \quad (7)$$

Pitta et al. (2009) classified the present model into two categories i) Amplitude modulated (AM), ii) Frequency Modulated (FM), depending upon the value of K_{ER} i.e. SERCA pump affinity to bind free Ca^{2+} . Here, $G_h(t)$ is zero mean, uncorrelated, Gaussian white-noise term with co-variance function (Nadkarni & Jung, 2007),

$$\langle G_h(t) G_h(t') \rangle = \frac{\alpha_h(1-h) + \beta_h h}{N_{\text{IP}_3}} \delta(t - t')$$

Here, $\delta(t)$ is the Dirac-delta function, t and t' are distinct times and $\frac{\alpha_h(1-h) + \beta_h h}{N_{\text{IP}_3}}$ is the spectral density (Coffey et al. 2005).

$$\begin{aligned} m_{\infty,a} &= \text{Hill}(p_a, d_1), \quad n_{\infty,a} = \text{Hill}(c_a, d_5), \quad \text{Hill}(x^n, K) = \frac{x^n}{x^n + K^n}, \\ h_\infty &= \frac{Q_2}{Q_2 + c_a}, \quad \tau_h = \frac{1}{a_2(Q_2 + c_a)}, \quad \text{and} \quad Q_2 = d_2 \frac{p_a + d_1}{p_a + d_3} \end{aligned}$$

h approaches its asymptotic value h_∞ with a time constant τ_h . Hill(x^n, K) is the generic Hill function (Pitta et al., 2009). Typically, Hill function is used for reactions whose intermediate steps are unknown (or not considered) but cooperative behavior is suspected in the reaction (Keener & Sneyd, 1998). Mathematically, it can be said that Hill function is used for reactions whose reaction velocity curve is not hyperbolic (Keener & Sneyd, 1998). Details of all parameters are as listed in Table 4.

Table 4: Parameters used for astrocyte Ca^{2+} dynamics

Symbol	Description	Value	Reference
r_{c_a}	Maximal IP ₃ R flux	6 s ⁻¹	Pitta et al. 2009
r_L	Maximal rate of Ca^{2+} leak from ER	0.11 s ⁻¹	Pitta et al. 2009
c_0	Total cell free Ca^{2+} concentration	2 μM	Pitta et al. 2009
$c_{1,a}$	Ratio of ER volume to cytosol volume	0.185	Pitta et al. 2009
v_{ER}	Maximal rate of SERCA uptake	0.9 $\mu\text{M s}^{-1}$	Pitta et al. 2009
K_{ER}	SERCA Ca^{2+} affinity	0.1 μM	Pitta et al. 2009
d_1	IP ₃ dissociation constant	0.13 μM	Pitta et al. 2009
d_2	Ca^{2+} inactivation dissociation constant	1.049 μM	Pitta et al. 2009
d_3	IP ₃ dissociation constant	0.9434 μM	Pitta et al. 2009
d_5	Ca^{2+} activation dissociation constant	0.08234 μM	Pitta et al. 2009
a_2	IP ₃ R binding rate for Ca^{2+} Inhibition	2 s ⁻¹	Pitta et al. 2009
N	Number of IP ₃ R in a cluster	20	Nadkarni & Jung, 2007
Glutamate-dependent IP ₃ production			
v_β	Maximal rate of IP ₃ production by PLC β	0.3 $\mu\text{M s}^{-1}$	Modified from Pitta et al. 2009
K_R	Glutamate affinity of the receptor	1.3 μM	Pitta et al. 2009
K_p	$\text{Ca}^{2+}/\text{PKC}$ -dependent inhibition factor	10 μM	Pitta et al. 2009
K_π	Ca^{2+} affinity of PKC	0.6 μM	Pitta et al. 2009
Glutamate-independent IP ₃ production			
v_δ	Maximal rate of IP ₃ production by PLC δ	0.02 $\mu\text{M s}^{-1}$	Pitta et al. 2009
$K_{\text{PLC}\delta}$	Ca^{2+} affinity of PLC δ	0.1 μM	Pitta et al. 2009
k_δ	Inhibition constant of PLC δ activity	1.5 μM	Pitta et al. 2009
IP ₃ degradation			
r_{5pa}	Maximal rate of degradation by IP-5P	0.04 s ⁻¹	Pitta et al. 2009
v_{3K}	Maximal rate of degradation by IP ₃ -3K	2 $\mu\text{M s}^{-1}$	Pitta et al. 2009
K_D	Ca^{2+} affinity of IP ₃ -3K	0.7 μM	Pitta et al. 2009
K_3	IP ₃ affinity of IP ₃ -3K	1 μM	Pitta et al. 2009

2.6 Glio-transmitter release dynamics in astrocyte

There is enough evidence that astrocytes actually release glio-transmitters in a Ca^{2+} dependent manner (Bezzi et al. 2004; Montana et al. 2006; Bowser & Khakh, 2007; Marchaland et al. 2008; Fellin, 2009). There is again considerable evidence that the released glio-transmitters modulate synaptic plasticity via extra-synaptic NMDAR (Parpura et al. 1994; Parpura & Haydon, 2000; Carmignoto & Fellin, 2006; Bergersen & Gundersen, 2009) and extra-synaptic mGluR (Fiacco & McCarthy, 2004; Perea & Araque, 2007). But, the exact mechanism by which astrocyte release glio-trasmitters is yet to be determined (Wenker, 2010). However, it is widely agreed upon that astrocytes release glio-transmitters in a vesicular manner similar to neurons (Bezzi et al. 2004; Montana et al., 2006; Verkhratsky & Butt, 2007; Marchaland et al. 2008). In 2000, Parpura & Haydon determined Ca^{2+} dependency of glutamate release from hippocampal astrocyte. The Hill co-efficient for glutamate release was 2.1 – 2.7, suggesting at least two Ca^{2+} ions are must for a possible glio-transmitter release. Thus, in this manuscript it has been assumed that binding of three Ca^{2+} ions leads to a release. It is assumed that release site contains three independent gates ($S_1 - S_3$) with different opening and closing constants. The model governing the glio-transmitter release probability closely follows Bertram et al. (1996) and is as follows,



Where, k_j^+ and k_j^- are the opening and closing rates of the gate ' S_j '; C_j and O_j are the closing and opening probability of gate S_j . The temporal evolution of the open gate ' O_j ' can be expressed as,

$$\frac{dO_j}{dt} = k_j^+ \cdot c_a - (k_j^+ \cdot c_a + k_j^-) \cdot O_j \quad (8)$$

The probability that a release site is activated is,

$$P_{ra} = O_1 \cdot O_2 \cdot O_3 \quad (9)$$

Similar to bouton, the vesicle fusion process is modeled using TMM with some modifications. The governing model is as follows,

$$\begin{aligned}
\frac{dR_a}{dt} &= \frac{I_a}{\tau_{rec}^a} - \Theta(c_a - c_a^{thresh}) \cdot P_{ra} \cdot R_a \\
\frac{dE_a}{dt} &= -\frac{E_a}{\tau_{inact}^a} + \Theta(c_a - c_a^{thresh}) \cdot P_{ra} \cdot R_a \\
I_a &= 1 - R_a - E_a
\end{aligned} \tag{10}$$

Here, ' R_a ' is the fraction of readily releasable Synaptic Like Micro-Vesicle (SLMV) inside the astrocyte, ' E_a ' is the fraction of effective SLMV in the extra-synaptic cleft and ' I_a ' is the fraction of inactive SLMV undergoing endocytosis or re-acidification process. ' Θ ' is the Heaviside function and ' c_a^{thresh} ' is the threshold of astrocyte $[Ca^{2+}]$ necessary for release site activation (Parpura & Haydon, 2000). τ_{inact}^a and τ_{rec}^a are the time constants of inactivation and recovery, respectively.

2.7 Glutamate dynamics in extra-synaptic cleft

The glutamate in the extra-synaptic cleft, g_a , has been modeled in a similar way to equation (6). This glutamate acts on extra-synaptically located mGluRs of the pre-synaptic bouton. It is used as an input in the IP_3 production term of equation (3). The SLMV of astrocytes are not as tightly packed as neurons (Bezzi et al., 2004). Thus, it is assumed that each SLMV contains 20 mM of glutamate (Montana et al., 2006). The mathematical equation governing glutamate dynamics are as follows,

$$\frac{dg_a}{dt} = n_a^v \cdot g_a^v \cdot E_a - g_a^c \cdot g_a \tag{11}$$

Where, g_a is the glutamate in the extra-synaptic cleft, ' n_a^v ' represents the SLMVs ready to be released, g_a^v is the glutamate concentration in one SLMV, g_a^c is the clearance rate of glutamate from the cleft due to diffusion and/or re-uptake.

Table 5: Parameters used for Glutamate dynamics in astrocyte and extra-synaptic cleft

Symbol	Description	Value	Reference
k_1^+	Ca^{2+} association rate for S_1	$3.75 \times 10^{-3} \mu M ms^{-1}$	Bertram et al. 1996
k_1^-	Ca^{2+} dissociation rate for S_1	$4 \times 10^{-4} ms^{-1}$	Bertram et al. 1996
k_2^+	Ca^{2+} association rate for S_2	$2.5 \times 10^{-3} \mu M ms^{-1}$	Bertram et al. 1996
k_2^-	Ca^{2+} dissociation rate for S_2	$1 \times 10^{-3} ms^{-1}$	Bertram et al. 1996
k_3^+	Ca^{2+} association rate for S_3	$5 \times 10^{-3} \mu M ms^{-1}$	Adjusted

k_3^-	Ca ²⁺ dissociation rate for S ₃	$1 \times 10^{-3} \text{ ms}^{-1}$	Assumed
$\tau_{\text{rec}}^{\text{a}}$	Vesicle recovery time constant	800 ms	Tsodyks & Markram, 1997
$\tau_{\text{inac}}^{\text{a}}$	Vesicle inactivation time constant	3 ms	Tsodyks & Markram, 1997
c_a^{thresh}	Astrocyte response threshold	196.69 nM	Parpura & Haydon, 2000
n_a^v	SLMV ready to be released	6	Assumed
g_a^v	Glutamate concentration in one SLMV	20 mM	Montana et al. 2006
g_a^c	Glutamate clearance rate from the extra-synaptic cleft	10 ms^{-1}	Destexhe et al. 1998

2.8 Dendrite Spine-head dynamics

The dendrite spine head is assumed to be of mushroom type. Its volume is taken to be $0.5242 \mu\text{m}^3$ (Koch, 1999). The specific capacitance and specific resistance of the spine head is assumed to be $1 \mu\text{F} / \text{cm}^2$ and $10000 \Omega \text{ cm}^2$, respectively. Given the dimensions of the spine we can calculate its actual resistance as,

$$R_m = \frac{R_M}{A_{\text{spine}}}$$

Where, R_m is actual resistance, R_M is specific resistance and A_{spine} is the area of spine head. NMDAR (N-methyl D-aspartate receptor) and AMPAR (α -amino-3-hydroxy-5-methyl-4-isoxazolepropionic acid receptor) are co-localized at most of the glutamatergic synapses, most of which are found at dendrite spines (Franks et al., 2002). Chen & Diamond (2002) showed that NMDAR receive less glutamate during evoked synaptic response, suggesting that most of the post-synaptic current is contributed by AMPAR, under such conditions. NMDARs are also known to play a crucial role in longer forms of synaptic plasticity, Long-term Potentiation (LTP) and Long-term Depression (LTD) (Bliss & Collingridge, 1993; Malenka & Bear, 2004). Hence, in our model the post-synaptic density comprises of AMPAR alone. The post-synaptic potential change has been modeled using a passive membrane mechanism (Tsodyks & Markram, 1997),

$$\tau_{\text{post}} \frac{dV_{\text{post}}}{dt} = -(V_{\text{post}} - V_{\text{post}}^{\text{rest}}) - R_m \cdot I_{\text{AMPA}} \quad (12)$$

Where, τ_{post} is the post-synaptic membrane time constant, $V_{\text{post}}^{\text{rest}}$ is the post-synaptic resting membrane potential, I_{AMPA} is the AMPAR current and is given by the following expression,

$$I_{\text{AMPA}} = g_{\text{AMPA}} m_{\text{AMPA}} (V_{\text{post}} - V_{\text{AMPA}})$$

Where, g_{AMPA} is the conductance of the AMPAR channel, V_{AMPA} is the reversal potential of the AMPAR and m_{AMPA} is the gating variable of AMPAR. Although there exists a more comprehensive 6-state markov model for AMPAR gating (Destexhe et al., 1998). In our model we have used a simple 2-state model for AMPAR gating. This two state model has been used keeping in mind it is computationally less expensive, while retaining the most of the important qualitative properties (Destexhe et al., 1998). Also, it is known that detailed AMPAR mechanisms like desensitization do not play a role in STP (Zucker & Regehr, 2002). AMPAR gating is governed by the following HH-type formulism (Destexhe et al., 1998),

$$\frac{dm_{\text{AMPA}}}{dt} = \alpha_{\text{AMPA}} g (1 - m_{\text{AMPA}}) - \beta_{\text{AMPA}} m_{\text{AMPA}}$$

Here, α_{AMPA} is the opening rate of the receptor, β_{AMPA} is the closing rate of the receptor and g is the glutamate concentration in the cleft given by equation (6). The parameter values are as listed in Table 6.

Table 6: List of parameters used for post-synaptic potential generation

Symbol	Description	Value	Reference
R_m	Actual resistance of the spine head	$3.18 \times 10^5 \text{ M}\Omega$	Calculated
$V_{\text{post}}^{\text{rest}}$	Post-synaptic resting membrane potential	-70 mV	Assumed
τ_{post}	Post-synaptic membrane time constant	10 ms	Calculated
g_{AMPA}	AMPAR conductance	1 nS	Destexhe et al. 1998
V_{AMPA}	AMPAR reversal potential	0 mV	Destexhe et al. 1998
α_{AMPA}	AMPAR forward rate constant	$1.1 \mu\text{M s}^{-1}$	Destexhe et al. 1998
β_{AMPA}	AMPAR backward rate constant	190 s^{-1}	Destexhe et al. 1998

2.9 Numerical Implementation

All the computations and visualizations of the model are implemented in MATLAB environment. The model equations were discretized with a temporal precision of, $\Delta t = 0.05$ ms. The canonical explicit Euler method was used to solve a system of twenty-two ordinary differential equations (equations 1 – 12). For the numerical simulation of the noise term, in equation (7), we have used Box-Muller Algorithm (Fox, 1997) to generate noise-term at each time-step (Δt). All simulations were performed on a Dell precision 3500 workstation with Intel Xeon processor with 2.8 GHz processing speed and with 12

GB (3 GB working) memory. The time taken for model time of 150s (stimulation rate 5 Hz) is approximately 885 sec. The MATLAB script written for the simulation of the model is supplied with the Supporting Material.

3. Simulation results

How post-synaptic current is being generated without the participation of astrocytic Ca^{2+} and with the participation of it (Figure 2), have been shown in this section with extensive numerical simulations of the model equations presented in the previous section. In the latter case how the output signal is being amplified through a processing loop, consisting of feed-forward and feed-back paths, with the help of astrocytic Ca^{2+} signaling, has been shown in Figure 2(B). Here, we have tried to answer the question, if astrocyte plays an active role in modulation of synaptic activity. In order to study the difference in both type of processing (see Figure 2), first we present the results associated with astrocyte-independent processing followed by astrocyte-dependent processing.

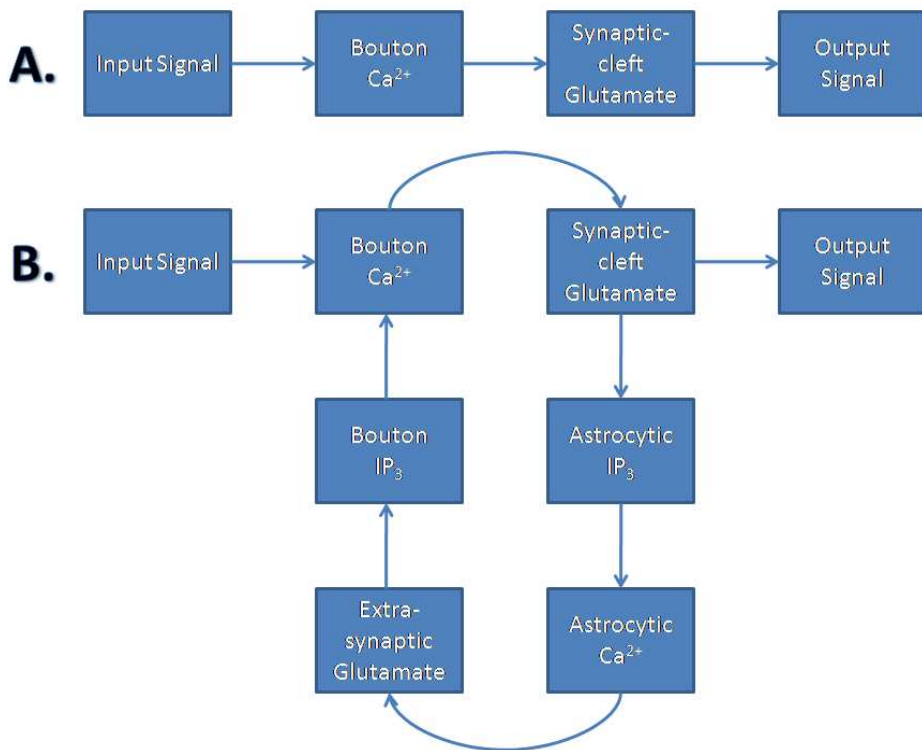


Figure 2. The two type of information processing simulated in this manuscript. (A) Astrocyte-independent information processing. (B) Astrocyte-dependent information processing, where, the input signal is being amplified by astrocyte-dependent feed-forward and feed-back pathways making up a loop.

3.1 Astrocyte-independent Information Processing

In this subsection we simulate the processing elaborated in Figure 2(A). We present results of implementation of the models described in subsections 2.1, 2.2, 2.4 and 2.8 (Figures 3(A), 3(B), 3(C), 3(D) and 3(E) respectively).

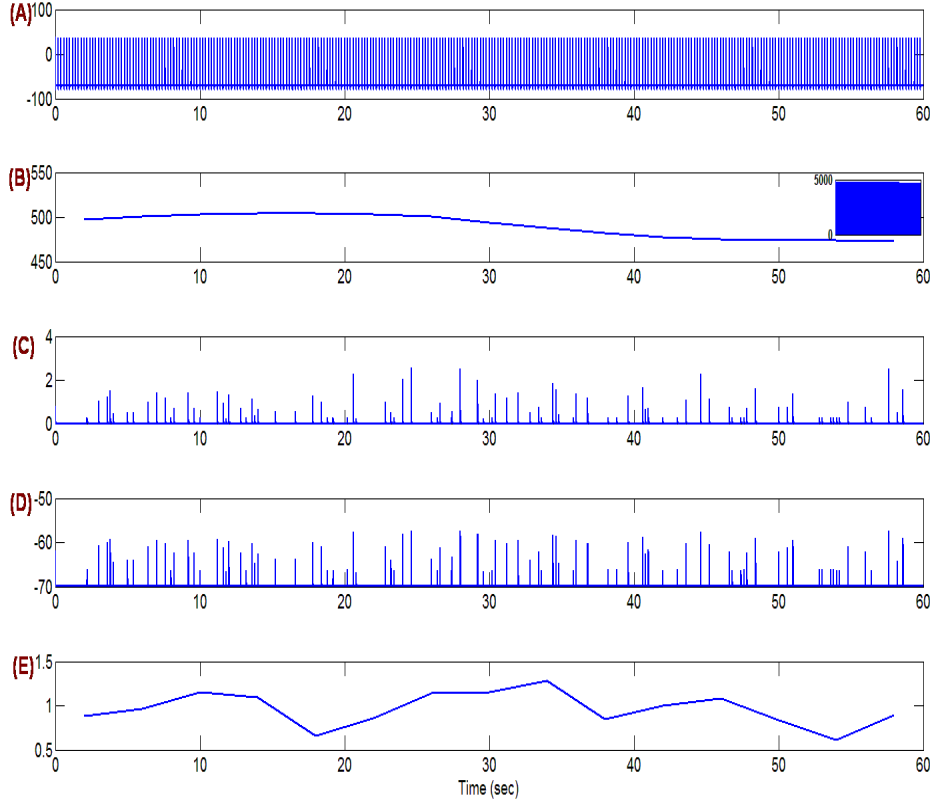


Figure 3. The major variables involved in astrocyte-independent information processing. (A) V_{pre} (mV); 5 Hz input signal generated using HH model, in response to a stimulus of $10 \mu\text{Acm}^{-2}$ of frequency 5 Hz and duration 10 ms. (B) $\langle \text{Ca}^{2+} \rangle$ (nM); Change in bouton Ca^{2+} averaged over a time-window of length 4 sec. In the inset is shown fast Ca^{2+} oscillation. (C) **Synaptic Glutamate** (mM); Elevated glutamate concentration in the synaptic cleft due to exocytosis of glutamate filled synaptic vesicles from bouton. (D) **Excitatory Post-Synaptic Potential (EPSP)** (mV); generated in response to an input signal (Figure 3(A)) using equation (12). (E) **Synaptic efficacy**; we have first averaged the Excitatory Post-Synaptic Current (EPSC) over a time-window of length 4 sec and then measured its relative change from its mean.

We used the model described in equation (1) to generate input signal or pre-synaptic membrane potential. This input signal forms the basis of signal transduction and we made sure that the system is at rest in its absence. In response to this input signal, the N-type Ca^{2+} channels open and bouton Ca^{2+} starts undergoing very fast oscillations (see inset of Figure 3(B)). Please note that, here, there is no astrocyte present and hence there is no contribution of $[\text{Ca}^{2+}]$ from intracellular stores. We preferred to show the change in average Ca^{2+} concentration ($\langle \text{Ca}^{2+} \rangle$) rather than fast changing Ca^{2+} because it is this average Ca^{2+} concentration of bouton which goes-up during opening of IP₃Rs on the intracellular stores. $\langle \text{Ca}^{2+} \rangle$ has been averaged using a time-window of length 4 sec. The only reason behind the choice of window length was to use the same window length as that used to show synaptic efficacy (see Figure 3(E)). We adjusted the number of Ca^{2+} channels so that the amplitude of Ca^{2+} oscillation is 5 μM i.e. exactly half of the affinity of Ca^{2+} sensor (β/α , where β and α are given in Table 3). Increased bouton $[\text{Ca}^{2+}]$

instigates the process of exocytosis and vesicles release their content (glutamate) in the synaptic cleft (see Figure 3(C)). When glutamate concentration rises in the cleft, it binds with post-synaptic AMPAR, which causes this ligand-gated channel to open. Once opened, AMPAR causes a change in the post-synaptic potential (see Figure 3(D)), since this, deflection is positive it has been termed as EPSP. Synaptic plasticity or synaptic efficacy is basically a measure of signal transduction success or failure. As a measure of synaptic efficacy, we measured mean amplitude of Excitatory Post-Synaptic Current (EPSC) (Perea & Araque, 2007), using a time-window of 4 sec. The notion behind using a time-window of 4 sec was that the effect of astrocyte was clearer using it. As described in the previous section, we also keep track of the vesicle recycling process (see equation (5)) which is shown in Figure 4.

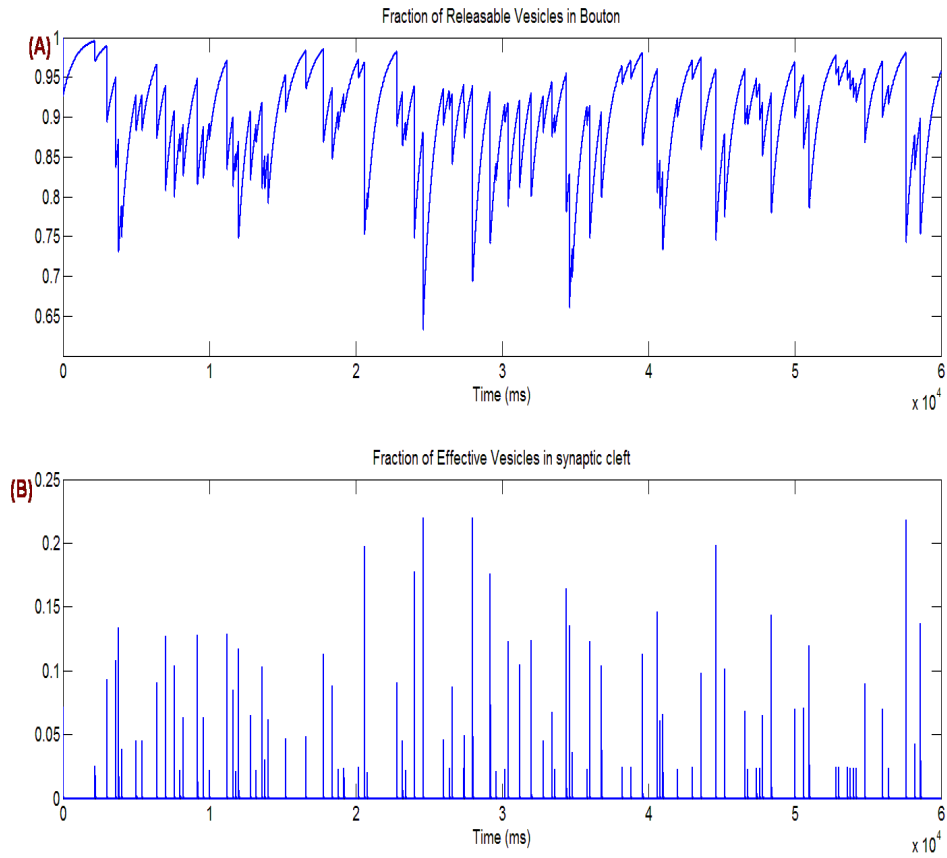


Figure 4. Fraction of releasable and effective vesicles, in astrocyte-independent information processing, during an input signal of 5 Hz (see Figure 3A). (A) The fraction of releasable vesicles i.e. ready to be fused, inside the bouton. (B) The fraction of effective vesicles i.e. fraction of vesicles fused and vesicles already in the synaptic cleft.

In Figure 4 we show the underlying process of vesicle release. In the absence of astrocyte, it can be observed that nearly 90% of the vesicles are available for release for most of the time (see Figure 4(A)). In Figure 4(B), we observe that the fraction of

effective vesicles is not as dense as the input signal (see Figure 3(A)) implying low probability of vesicle release. In fact, the probability of vesicle release was nearly 0.3 i.e. every third input signal is able to release a synaptic vesicle.

3.2 Astrocyte-dependent Information Processing

In this sub-section, we show simulations associated with the phenomenological model governed by equations (1 – 12) i.e., the astrocyte-dependent information processing. In Figure 5, we give an idea of the processes involved in the loop shown in Figure 2(B). For the simulation of the scheme, shown in Figure 2(B), we simultaneously solved equations (1 – 12). Of particular interest is the astrocyte-dependent feed-forward and feed-back paths making up a loop (Figure 2(B)). The same input signal was used in a feed-back manner into the loop. It may amplify the input signal leading to enhanced synaptic efficacy.

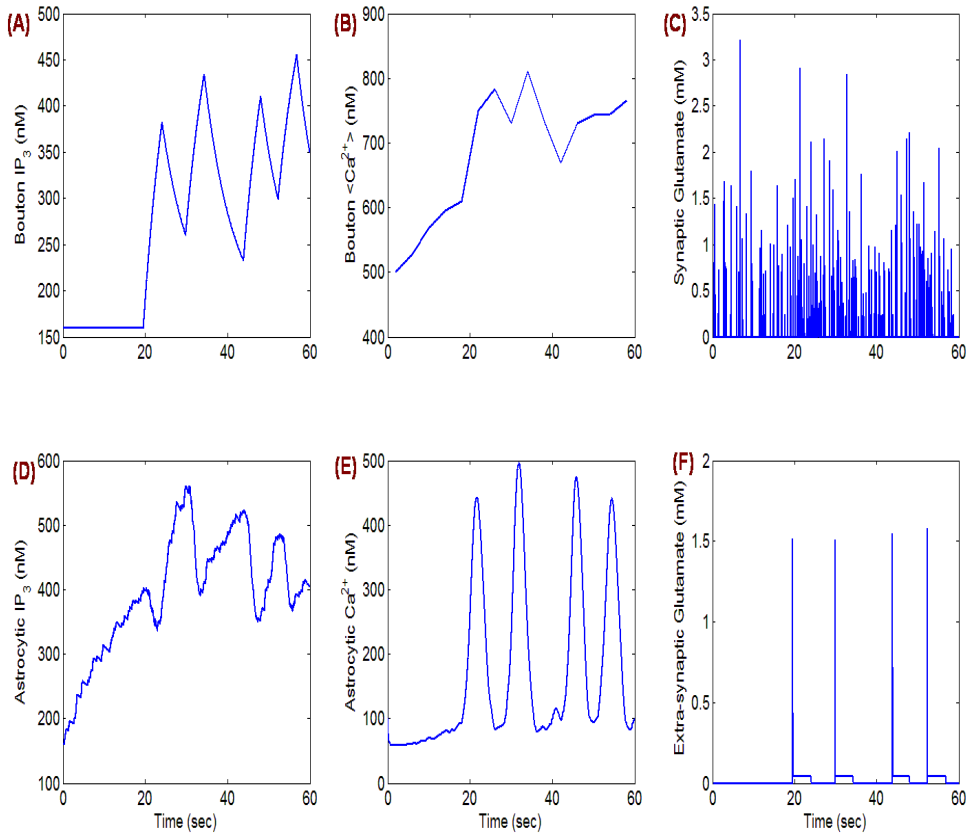


Figure 5. The major variables involved in astrocyte-dependent information processing. Here, input signal is same as Figure 3 and is omitted. Synaptic efficacy is also generated and measured in a similar way (see Figure 3D) is omitted only to show comparison in Figure 7. (A) Increased bouton IP_3 concentration in response to elevated extra-synaptic glutamate concentration (see Figure 5F). (B) Increased IP_3

concentration causing the IP₃R channel to open and leading to an increase in average bouton Ca²⁺, due to influx of Ca²⁺ from IP₃R. (C) Accumulated bouton [Ca²⁺] leads to increased transients of glutamate concentration in the synaptic cleft. (D) Increased transients of glutamate concentration set-off the production of astrocytic IP₃ concentration through an mGluR dependent pathway. (E) Elevated astrocytic IP₃ concentration cause the IP₃R channel to open and initiate astrocyte Ca²⁺ oscillations. (F) Astrocyte Ca²⁺ oscillations instigate the process of SLMV fusion which is followed by a raised extra-synaptic glutamate concentration. This elevated extra-synaptic glutamate concentration forms the basis of bouton IP₃ production shown in Figure 5A.

All the variables shown in Figure 5 are inter-dependent i.e., variation in one affects variation in others. When the bouton is fed with an input signal, it shows its response, in the form of increased cytosolic [Ca²⁺]. This elevated [Ca²⁺] exocytose glutamate in the synaptic cleft (see Figure 5(C)). After being exocytose, synaptic glutamate has two fates (see Figure 2(B)). It can bind with post-synaptic AMPAR and it can bind with mGluR on the surface of the astrocyte. Once this glutamate binds with mGluR, it instigates the production of astrocytic IP₃ (see Figure 5(D)) through a G-protein link. During this glutamate spill-over process astrocytic IP₃ concentration goes on appreciating and gradually starts oscillating. It can be observed from Figure 5D and Figure 5E that astrocytic Ca²⁺ also starts oscillating, as soon as, astrocytic IP₃ starts oscillating. Although, the biological significance and importance of IP₃ oscillation on Ca²⁺ oscillation is not clearly understood (Pitta et al., 2009). This astrocytic Ca²⁺ is known to exocytose SLMV filled with glutamate once it crosses its threshold value of 196.69 nM (Parpura & Haydon, 2000). Similarly, whenever astrocyte Ca²⁺ crosses its threshold value it can spill glutamate, contained in SLMV, in the extra-synaptic cleft (see Figure 5E). We have mathematically modeled this process of astrocyte glutamate release using equations (8 – 11). Extra-synaptic glutamate binds with extra-synaptic mGluRs located on the surface of the bouton, and initiates the production of bouton IP₃ (see Figure 5A) through a G-protein link. It is visible from Figure 5E and Figure 5A that bouton IP₃ production starts only when astrocyte spills glutamate in the extra-synaptic cleft, reflecting the significance of extra-synaptic glutamate in the model. This bouton IP₃ is free to diffuse inside the cytosol and opens the IP₃R on the intracellular stores in a Ca²⁺-dependent manner. Similar to the previous sub-section, we have shown $\langle \text{Ca}^{2+} \rangle$ instead of showing the fast Ca²⁺ oscillations. Unlike previous observation of $\langle \text{Ca}^{2+} \rangle$, we can see accumulation of Ca²⁺ inside the bouton (increasing $\langle \text{Ca}^{2+} \rangle$). This accumulation of Ca²⁺ is as a result of opening IP₃Rs on the surface of the intracellular store. Flow of Ca²⁺ through this IP₃R is a slow process and is known to play a crucial role in modulating synaptic plasticity and spontaneous vesicle release (Emptage et al., 2001).

The synaptic vesicle exocytosis from bouton and SLMV release from astrocyte has been modeled using equations (4 – 5) and equations (8 – 10), respectively. Figure 6A and Figure 6B show the fraction of releasable and effective vesicles during synaptic vesicle recycling process emulated using equations (4 – 5). Figure 6A and 6B are similar to the

diagrams in Figure 4, except the astrocyte-dependent pathway. The SLMV recycling process has been modeled using equation (10).

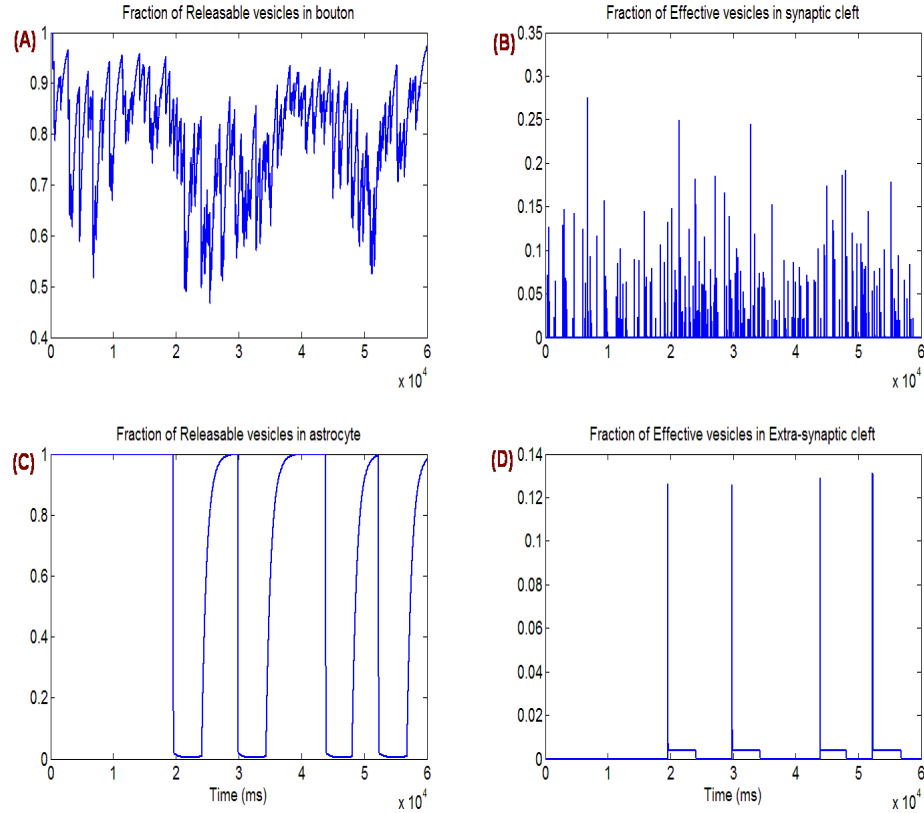


Figure 6. Fraction of releasable and effective vesicles, in astrocyte-dependent information processing, during an input signal of 5 Hz (see Figure 3A). (A) Fraction of releasable vesicles inside the bouton. (B) Fraction of effective vesicles in the synaptic cleft i.e. fraction of vesicles fused and residual vesicles in the synaptic cleft. (C) Fraction of releasable SLMVs inside the astrocyte. (D) Fraction of effective SLMVs in the extra-synaptic cleft.

Figure 6C and Figure 6D show the fraction of releasable vesicles in astrocyte and effective vesicles in extra-synaptic cleft. It can be observed from Figure 6A that more than 80% of the releasable (docked) vesicles have been used in astrocyte-dependent pathway. Also, the fraction of effective vesicles in the synaptic cleft has also considerably gone-up (compare with Figure 4B). It is because of the increased $\langle \text{Ca}^{2+} \rangle$ which improves synaptic vesicle release probability. In fact, the vesicle release probability during this pathway was nearly, 0.8, implying four out of five spikes are able to release a synaptic vesicle.

3.3 Comparison between the two-forms of information processing

In this subsection, we have undertaken a comparative study between the two forms of information processing (see Figure 2A & 2B). We will discuss some of our findings

keeping in mind the recent controversy regarding whether astrocytic Ca^{2+} can contribute in synaptic plasticity or not (e.g., Henneberger et al., 2010 vs. Agulhon et al., 2010).

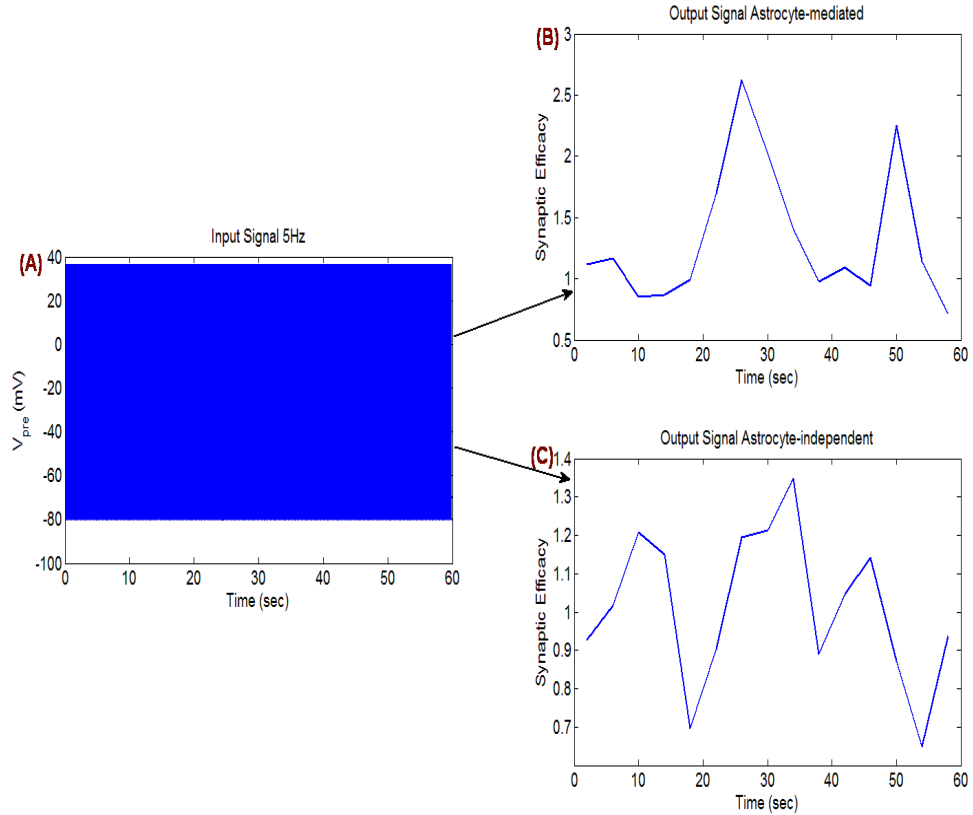


Figure 7. A comparison of the two modes of information processing (see Figure 2) in response to the same input signal of 5 Hz. The measure of synaptic efficacy is calculated as described in text. Here, the black arrows enclose the details shown and described for astrocyte-independent and astrocyte-dependent information processing (see Figure 3 – 6). (A) Input signal of 5 Hz, (B) Output signal using astrocyte-dependent information processing and (C) Output signal using astrocyte-independent information processing.

Using their experimental setup Perea & Araque (2007) demonstrated an increase in synaptic efficacy, at single CA3 – CA1 synapse, during the phase of high astrocyte $[\text{Ca}^{2+}]$ (see Figure 1F). They stimulated the pre-synaptic neuron and simultaneously, increased the astrocyte $[\text{Ca}^{2+}]$ through different pathways, e.g., purinergic receptors (P2Y-R), and recorded the EPSCs. In particular they used caged Ca^{2+} and used UV-flash to artificially increase astrocytic $[\text{Ca}^{2+}]$. In contrast, in our mathematical model, we allow an activity-dependent increase in astrocytic IP_3 following an AP. As a measure of change in synaptic strength, synaptic efficacy, they demonstrated an increase in mean EPSC amplitude when astrocyte was stimulated. We measured the mean EPSC after every 4 sec. In Figure 7B, the mean EPSCs have been measured relative to the mean EPSC during first 20 sec (see

Figure 7B & 7C), because it is the phase during which astrocyte Ca^{2+} has not exceeded its threshold (see Figure 3E). In Figure 7C, the mean EPSCs have been measured relative to their overall mean. Please note that, Figure 7C is same as Figure 3E, but has been shown for comparison purpose. The impact of astrocyte response is clearly visible when we look at Figure 7B & 7C. In astrocyte-independent information flow, there is not much deviation ($\pm 30\%$) from its mean value, while in astrocyte-dependent information flow there is a transient increase of nearly 250%. This increase is subsequent to the rise in astrocytic Ca^{2+} (see Figure 3E) and has decay time constant, the time necessary to decay to $1/e$ of its initial magnitude (Fisher et al, 1997), of nearly 10s. This increase in synaptic efficacy falls under short-term-enhancement, in particular augmentation, given the classification in Koch (1999, p – 311).

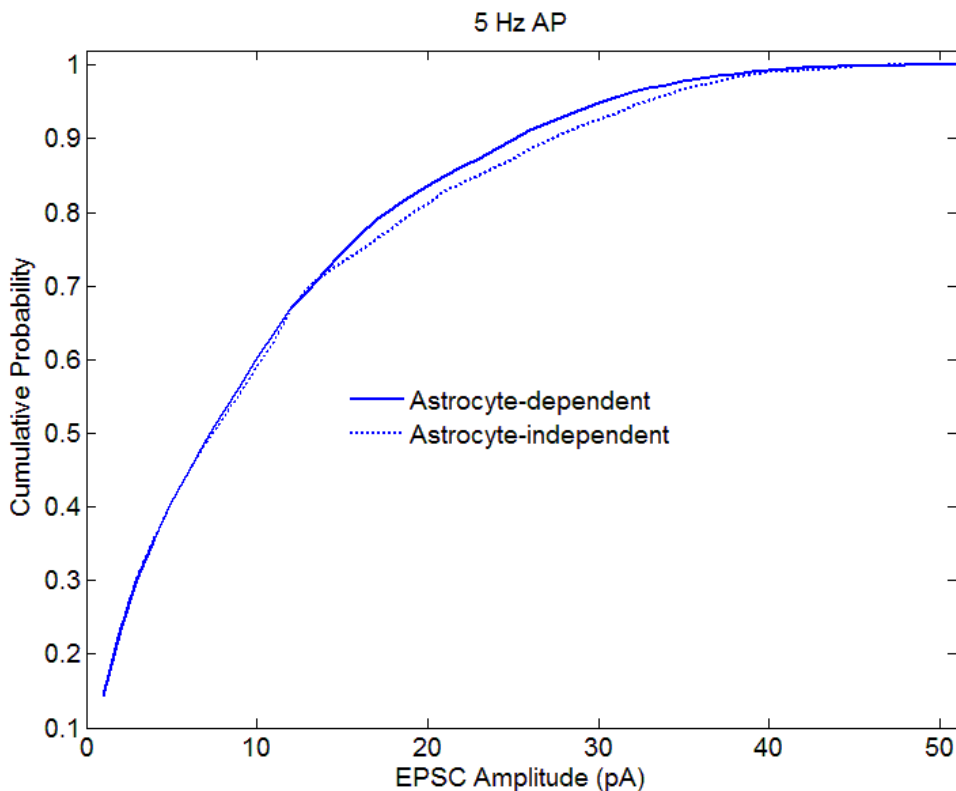


Figure 8. Cumulative probability of EPSC amplitude in response to an input signal of 5 Hz. Astrocyte-dependent curve shifts upwards implying an increased probability of having EPSC amplitude between 15 to 30 pA.

Perea & Araque (2007) also demonstrated an increase in cumulative probability of EPSC amplitude before (astrocyte-independent) and during (astrocyte-dependent) astrocyte stimulation (see Figure 1E, Perea & Araque, 2007). Similar to their experimental observations, we also observed an increase in probability of EPSC amplitude (see Figure 8). This implies that there are more chances of having EPSC amplitude between 15 to 30 pA when astrocyte is present. It is not a good idea to demonstrate an enhancement in

synaptic efficacy. As, we observed that, for an input signal of 10Hz and 20Hz the situation remains the same and the impact of astrocyte becomes more prominent, while, for an input signal of 2Hz the situation was vice-versa (data not shown). A more comprehensive way of demonstrating synaptic enhancement will be to show that we have more number of post-synaptic events in astrocyte-dependent processing than astrocyte-independent processing. In Figure 9, we show cumulative probability for inter-arrival time of post-synaptic potentials. It is visible from the figure that the probability of having post-synaptic potentials in short durations has greatly increased in presence of astrocyte (see Figure9).

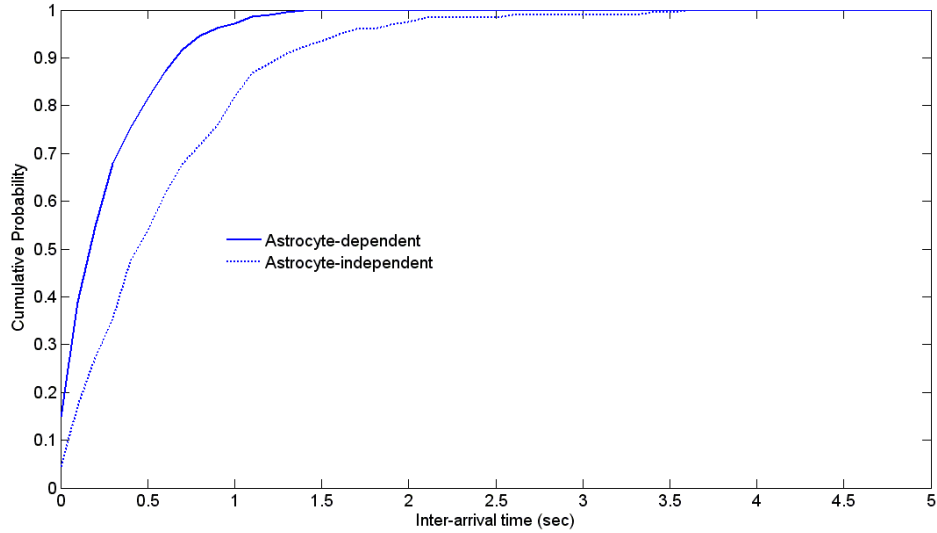


Figure 9. Cumulative probability distribution of inter-arrival time of Excitatory Post-Synaptic Potential (EPSP) for astrocyte-dependent and astrocyte-independent information processing. The distribution associated with astrocyte-dependent process shifts radically to the left suggesting reduced inter-arrival time due to enhanced synaptic efficacy.

During this type of astrocyte-induced plasticity, it is known that synaptic potency remains unchanged (Perea & Araque, 2007). Synaptic potency is given as a measure of mean post-synaptic potential response, excluding failures. We calculated the mean of each successful post-synaptic response in a time-window of 5 sec. It can be observed from Figure 10 that there is no apparent difference in synaptic potency under both forms of information processing. This observation was also confirmed statistically using a two-sample student's t-test. Synaptic potencies were assumed to be independent random samples. It was tested that both samples are from normal distributions with equal mean and equal but unknown variances (*null hypothesis*), against the alternative that the means are not equal with 5% significance level. The result returned a *p*-value of 0.5543 indicating a failure to reject null hypothesis.

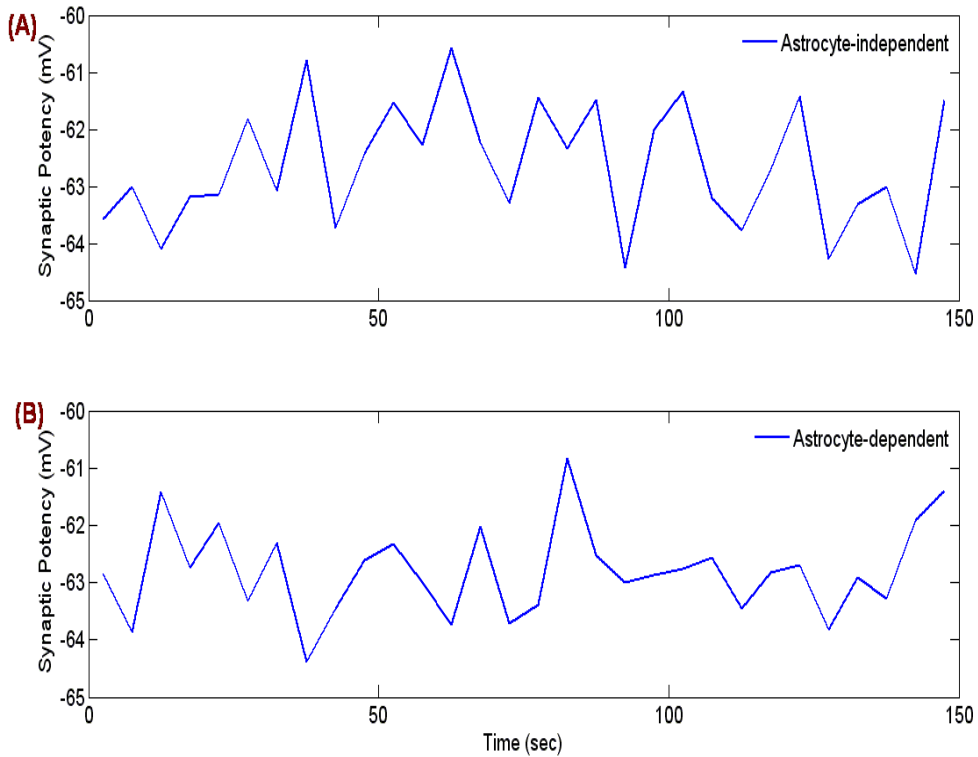


Figure 10. Synaptic potency under both forms of information processing (i.e. astrocyte-independent & astrocyte-dependent). Synaptic efficacy is given as a measure of mean EPSP, calculated over a time-window of 5-sec, excluding failures. Synaptic potency is unchanged in both cases which has also been observed in recent experiments (see Figure 1 of Perea & Araque (2007)); (A) mean = -62.7979 mV, std = 0.8039 mV; (B) mean = -62.6503 mV, std = 1.0956 mV. The two-sample paired t-test also confirms the previous statement ($p = 0.5543$).

4. Conclusion and future directions

There is a raging debate regarding the mechanism and calcium dependence of gliotransmission and the role of gliotransmission in synaptic plasticity. Together they imply that effect of astrocytic calcium on synaptic plasticity is a controversial issue. Here we have put together a number of phenomenological models for the processes shown in Figure 2 to simulate the effects on synaptic strength with and without astrocytic Ca^{2+} . From the computational modeling point of view this is equivalent to controlling the effect of Ca^{2+} in astrocytes by genetic engineering (Agulhon et al., 2010) and by calcium clamp (Henneberger et al., 2010) in order to study the effects of astrocytic Ca^{2+} on synaptic plasticity. A better understanding, through varieties of approaches, of calcium dynamics, signaling and gliotransmitter release is necessary for settling down the aforementioned debate (Ben Achour et al., 2010). Here we have taken a computational approach, and concluded that the astrocytic Ca^{2+} contributes to the synaptic augmentation at the seconds time scale.

We have presented a mathematical model which studies the effect of astrocyte over the hippocampal CA3-CA1 synaptic strength. It is found that given the pathway (Figure

2B), astrocyte plays a significant role in modulating synaptic information transfer. It might be possible that under physiological conditions, neurons also exhibit the two types of information processing: i) astrocyte-independent ii) astrocyte-dependent. It is suggested that neurons process information usually in astrocyte-independent manner unless there is some learning or memory activity to be processed. It is worth mentioning here that, it is not possible to conclude and assert that astrocyte induces a particular type of synaptic plasticity (e.g. augmentation) using only a temporal model, proposed here, as synaptic plasticity depends on several spatial constraints. As a future direction, it is proposed to develop a spatio-temporal model to study the effect spatial constraints, like release sites, Ca^{2+} source etc., over modulation of synaptic activity. It is also known that a single hippocampal astrocyte in CA1 region ensheathes around thousands of synapses (Schipke & Peters, 2009). Thus, it is possible for a single astrocyte to modulate signal processing at thousands of synapses. It has also been shown, experimentally that, astrocyte helps in synchronized activity of neurons in CA1 region (Carmignoto & Fellin, 2006). Hence, it is proposed to study the effect of astrocyte over the networks of neurons. The present mathematical model is quite adaptable and can be easily extended to study longer and other forms of synaptic plasticity.

Another advantage of this model is that it can be extended to astrocyte microdomains, where it is difficult to experimentally manipulate calcium fluctuations. Simply increasing intracellular calcium is not sufficient for gliotransmitter release, as evident from conflicting results (Henneberger et al., 2010; Agulhon et al., 2010; Wenker, 2010). If calcium is truly required for transmitter release, then it may need to occur in specific microdomains (Wenker, 2010), which has been over-looked and needs examination using similar computational modeling approach.

Acknowledgments

The work has been supported by the Department of Science and Technology, Government of India, grant no. SR/CSI/08/2009. Helpful suggestions from Vladimir Parpura are being thankfully acknowledged.

References

- Agulhon, C., Fiacco, T. A., & McCarthy, K. D. (2010). Hippocampal short- and long-term plasticity are not modulated by astrocyte Ca^{2+} signaling. *Science*, 327, 1250 – 1254.
- Andersson, E. H. (2010). Astrocytes impose postburst depression of release probability at hippocampal glutamate synapses. *J. Neurosci.*, 30(16), 5776 – 5780.
- Araque, A., Parpura, V., Sanzgiri, R. P., & Haydon, P. G. (1999). Tripartite synapses: glia, the unacknowledged partner. *Trends Neurosci.*, 22, 208 – 215.
- Ben Achour, S., Pont-Lezica, L., Bechade, C., & Pascual, O. (2010). Is astrocyte calcium signaling relevant for synaptic plasticity? *Neuron Glia Biol.*, 6(3), 147 – 155.
- Blackwell, K. T. (2005). Modeling Calcium Concentration and Biochemical Reactions. *Brains, Minds, and Media*, 1, 1 – 27.

- Bergersen, L. H. & Gundersen, V. (2009). Morphological Evidence For Vesicular Glutamate Release From Astrocytes. *Neuroscience*, 158, 260–265.
- Bertram, R., Sherman, A. & Stanley, E. F. (1996). Single-Domain/Bound Calcium Hypothesis of Transmitter Release and Facilitation. *J. Neurophys.*, 75, 1919 – 1931.
- Bezzi, P., Gundersen, V., Galbato, J. L., Seifert, G., Steinhauser, C., Pilati, E., & Volterra, A. (2004). Astrocytes contain a vesicular compartment that is competent for regulated exocytosis of glutamate. *Nature Neurosci.*, 7, 613 – 620.
- Bliss, T. V. P. & Collingridge, G. L. (1993). A synaptic model of memory: long-term potentiation in the hippocampus. *Nature*. 361, 31 – 39.
- Bollmann, J. H., Sakmann, B., Borst, J. G. G. (2000). Calcium Sensitivity of Glutamate Release in a Calyx-Type Terminal. *Science*. 289, 953 – 957.
- Bowser, D. N. & Khakh, B. S. (2007). Two forms of single-vesicle astrocyte exocytosis imaged with total internal reflection fluorescence microscopy. *PNAS*, 104, 4212–4217.
- Cajal, R. Y. (1913). *Histologie du systeme nerveux de l'homme et des vertebres*. Maloine, Paris.
- Carmignoto, G. & Fellin, T. (2006). Glutamate release from astrocytes as a non-synaptic mechanism for neuronal synchronization in the hippocampus. *Journal of Physiology*, 99, 98–102.
- Chen, S. & Diamond, J. S. (2002). Synaptically Released Glutamate Activates Extrasynaptic NMDA Receptors on Cells in the Ganglion Cell Layer of Rat Retina. *The Journal of Neuroscience*, 22, 2165–2173.
- Coffey, W. T., Kalmykov, Yu., P., & Waldron, J. T. (2005). *The Langevin Equation: With Applications To Stochastic Problems In Physics, Chemistry And Electrical Engineering*, 2nd Edition. World Scientific Publishing, Singapore.
- Danbolt, N. C. (2001). Glutamate uptake. *Progress in Neurobiology*. 65, 1–105.
- Destexhe, A., Mainen, Z. F., & Sejnowski, T. J. (1998). Kinetic Models of Synaptic Transmission, in: *Methods in Neuronal Modeling*, Koch, C. & Segev, I., MIT Press, Cambridge, 1 – 25.
- Emptage, N. J., Reid, C. A., & Fine, A. (2001). Calcium Stores in Hippocampal Synaptic Boutons Mediate Short-Term Plasticity, Store-Operated Ca^{2+} Entry, and Spontaneous Transmitter Release. *Neuron*. 29, 197–208.
- Erler, F., Meyer-Hermann, M., Soff, G. (2004). A quantitative model for pre-synaptic free Ca^{2+} dynamics during different stimulation protocols. *Neurocomputing*. 61, 169 – 191.
- Fall, C., Marland, E., Wagner, J., & Tyson, J. (2002). *Computational Cell Biology*, Springer-Verlag, Newyork.
- Fellin, T. (2009). Communication between neurons and astrocytes: relevance to modulation of synaptic and network activity. *J. Neurochem*. 108, 533 – 544.
- Fiacco, T. A. & McCarthy, K. D. (2004). Intracellular Astrocyte Calcium Waves In Situ Increase the Frequency of Spontaneous AMPA Receptor Currents in CA1 Pyramidal Neurons. *The Journal of Neuroscience*, 24, 722–732.

- Fisher, S. A., Fischer, T. M., & Carew, T. J. (1997). Multiple overlapping processes underlying short-term synaptic enhancement. *Trends Neurosci.* 20, 170 – 177.
- Franks, K. M., Bartol, T. M., & Sejnowski, T. J. (2002). A Monte Carlo Model Reveals Independent Signaling at Central Glutamatergic Synapses. *Biophys. J.*, 83, 2333–2348.
- Fox, R. F. (1997). Stochastic Versions of the Hodgkin-Huxley Equations. *Biophys. J.*, 72, 2068-2074.
- Haydon, P. G. (2001). Glia: listening and talking to the synapse. *Nature Rev. Neurosci.* 2, 185 – 193.
- Hebb, D. O. (1949). *The organization of behavior*. Wiley, New York.
- Henneberger, C., Papouin, T., Oliet, S. H. R., & Rusakov, S. A. (2010). Long-term potentiation depends on release of D-serine from astrocytes. *Nature*. 463, 232 – 236.
- Hodgkin, A. L. & Huxley, A. F. (1952). A Quantitative Description Of Membrane Current And Its Application To Conduction And Excitation In Nerve. *J. Physiol.* 117, 500-544.
- Ishikawa, T., Kaneko, M., Shin, H-P & Takahashi, T. (2005). Pre-synaptic N-type and P/Q-type Ca^{2+} channels mediating synaptic transmission at the calyx of Held of mice. *J Physiol.* 568, 199–209.
- Jafri, M. S. & Keizer, J. (1995). On the Roles of Ca^{2+} Diffusion, Ca^{2+} Buffers, and the Endoplasmic Reticulum in IP_3 -Induced Ca^{2+} Waves. *Biophys. J.*, 69, 2139-2153.
- Jensen, T. P., Filoteo, A. G., Knopfel, T., & Empson, R. M. (2007). Pre-synaptic plasma membrane Ca^{2+} ATPase isoform 2a regulates excitatory synaptic transmission in rat hippocampal CA3. *J Physiol.* 579, 85–99.
- Keener, J. & Sneyd, J. (1998). *Mathematical Physiology*. Springer – Verlag, New York.
- Koch, C. (1999). *Biophysics of computation: information processing in single neurons*. Oxford University Press, New York.
- Koester, H. J. & Sakmann, B. (2000). Calcium dynamics associated with action potentials in single nerve terminals of pyramidal cells in layer 2/3 of the young rat neocortex. *J. Phys.*, 529, 625 – 646.
- Li, Y-X & Rinzel, J. (1994). Equations for IP_3 receptor mediated Ca^{2+} oscillations derived from a detailed kinetic model: A Hodgkin-Huxley like formulism. *J. theor. Biol.* 166, 461 – 473.
- Lynch, M. A. (2004). Long-term potentiation and memory. *Physiol. Rev.*, 84, 87 – 135.
- Lytton, W. W. & Sejnowski, T. J. (1991). Simulations of Cortical Pyramidal Neurons Synchronized by Inhibitory Interneurons. *J. Neurophys.*, 66, 1059 – 1079.
- Marchaland, J., Cali, C., Voglmaier, S. M., Li, H., Regazzi, R., Edwards, R. H., & Bezzi, P. (2008). Fast Subplasma Membrane Ca^{2+} Transients Control Exo-Endocytosis of Synaptic-Like Microvesicles in Astrocytes. *The Journal of Neuroscience*, 28, 9122–9132.
- Malenka, R. C. & Bear, M. F. (2004). LTP and LTD: An Embarrassment of Riches. *Neuron*, 44, 5–21.
- Mazzanti, M. & Haydon, P. G. (2003). Astrocytes Selectively Enhance N-Type Calcium Current In Hippocampal Neurons. *Glia*. 41, 128–136.

- Montana, V., Malarkey, E. B., Verderio, C., Matteoli, M., & Parpura, V. (2006). Vesicular Transmitter Release From Astrocytes. *Glia*, 54, 700–715.
- Nadkarni, S., & Jung, P. (2003). Spontaneous oscillations in dressed neurons: A mechanism for epilepsy? *Phys. Rev. Lett.*, 91, 268101-1 – 260181-4.
- Nadkarni, S. & Jung, P. (2007). Modeling synaptic transmission of the tripartite synapse. *Phys. Biol.* 4, 1–9.
- Nadkarni, S., Jung, P., & Levine, H. (2008). Astrocytes optimize the synaptic transmission of information. *PLoS Comp. Biol.*, 4(5), 1 – 11.
- Naundorf, B., Wolf, F., & Volgushev, M. (2006). Unique features of action potential initiation in cortical neurons. *Nature*, 440, 1060 – 1063.
- Neher, E. (1998). Vesicle Pools and Ca^{2+} Microdomains: New Tools for Understanding Their Roles in Neurotransmitter Release. *Neuron*. 20, 389–399.
- Newman, E. A. (2003). New roles for astrocytes: Regulation of synaptic transmission. *Trends Neurosci.*, 26(10), 536 – 542.
- Nikonenko, A. G. & Skibo, G. G. (2006). Age-Related Changes in Synaptic Vesicle Pools of Axo-Dendritic Synapses on Hippocampal Ca^{2+} Pyramidal Neurons in Mice. *Neurophysiology*. 38, 407 – 411.
- Parpura, V., Basarsky, T. A., Liu, F., Jeftinija, K., Jeftinija, S. & Haydon, P. G. (1994). Glutamate mediated astrocyte-neuron signaling. *Nature*, 369, 744–747.
- Parpura, V. & Haydon, P. G. (2000). Physiological astrocytic calcium levels stimulate glutamate release to modulate adjacent neurons. *Proc. Natl Acad. Sci.*, 97, 8629–8634.
- Perea, G., & Araque, A. (2002). Communication between astrocytes and neurons: a complex language. *J. Physiol. Paris.*, 96, 199 – 207.
- Perea, G., & Araque, A. (2007). Astrocytes potentiate transmitter release at single hippocampal synapses. *Science*. 317, 1083 – 1086.
- Pittà, M. De, Goldberg, M., Volman, V., Berry, H., & Ben-Jacob, E. (2009). Glutamate regulation of calcium and IP₃ oscillating and pulsating dynamics in astrocytes. *J Biol Phys.*, 35, 383 – 411.
- Schipke, C.G. & Peters, O. (2009). Glial Influence on Synaptic Transmission, in *Intercellular Communication In The Nervous System*, R.C. Malenka, ed., Elsevier, pp. 112 – 120.
- Schneggenburger, R. & Neher, E. (2000). Intracellular calcium dependence of transmitter release rates at a fast central synapse. *Nature*. 406, 889 – 893.
- Sneyd, J. & Falcke, M. (2005). Models of the inositol trisphosphate receptor. *Progress in Biophysics and Molecular Biology*. 89, 207–245.
- Tsodyks, M. & Markram, H. (1997). The neural code between neocortical pyramidal neurons depends on neurotransmitter release probability. *Proc. Natl. Acad. Sci. USA*. 94, 719–723.
- Verkhratsky, V. & Butt, V. (2007). *Glial Neurobiology: A Textbook*. John Wiley & Sons Ltd.

- Vernadakis, A. (1996). Glia-neuron intercommunications and synaptic plasticity. *Prog. Neurobiol.* 49, 185 – 214.
- Volman, V., Ben-Jacob, E., & Levine, H. (2007). The astrocytes as a gatekeeper of synaptic information transfer. *Neural Comp.*, 19, 303 – 326.
- Weber, A. M., Wong, F. K., Tufford, A. R., Schlichter, L. C., Matveev, V., & Stanley, E. F. (2010). N-type Ca^{2+} channels carry the largest current: implications for nanodomains and transmitter release. *Nature Neurosc.* 13, 1348 – 1350.
- Wang, L-Y, Fedchyshyn, M. J., & Yang, Y-M (2009). Action potential evoked transmitter release in central synapses: insights from the developing calyx of Held. *Molecular Brain*. 2, 1- 11.
- Wenker, I. (2010). An active role for astrocytes in synaptic plasticity? *J. Neurophysiol.* 104, 1216 – 1218.
- Wu, L., & Borst, J. G. G. (1999). The reduced release probability of releasable vesicles during recovery from short-term synaptic depression. *Neuron*. 23(4), 821 – 832.
- Yang, Y., Ge, W., Chen, Y., Zhang, Z., Shen, W., Wu, C., Poo, M., & Duan, S. (2003). Contribution of astrocytes to hippocampal long-term potentiation through release of D-serine. *PNAS*. 100(25), 15194 – 15199.
- Zucker, R. S., & Regehr, W. G. (2002). Short-term synaptic plasticity. *Annu. Rev. Physiol.*, 64, 355 – 405.